Intracellular Control of Axial Shape in Non-uniform Neurites: A Serial Electron Microscopic Analysis of Organelles and Microtubules in AI and AII Retinal Amacrine Neurites

SHARON E. SASAKI-SHERRINGTON, J. ROGER JACOBS, and JOHN K. STEVENS
Playfair Neuroscience Unit, University of Toronto, Toronto Western Hospital, Toronto, Ontario, Canada

ABSTRACT AI and AII cat retinal amacrine cells have highly varicose non-uniform, neuritic processes. Processes of both types were reconstructed via a computer system using serial electron micrographs. These reconstructions were analyzed for (a) varicosity volume, surface area, and length, (*b*) "neck" volume, surface area, and length, (*c*) number of microtubules within the varicosity, (*d*) number of microtubules within the "neck," and (e) volume and surface area of mitochondria and smooth endoplasmic reticulum and large smooth vesicular bodies within the processes. Correlation of these parameters revealed a linear relationship between the number of microtubules in the necks and mean neck cross-sectional area (r_S = 0.780, $P < 0.001$), while microtubule number within the varicosities showed no correlation with varicosity volume ($r_S = 0.239$, $P > 0.2$). Varicosity volume did, however, correlate strongly with the summed volume of mitochondria and smooth vesicular bodies contained within the varicosity for both cell types examined. The ratio between membranous organelle volume and varicosity volume for AI amacrine processes of 1:6.97 ($r_S = 0.927$), differed from the ratio of 1:1.80 for the AII amacrine processes ($r_S = 0.987$). Similar relationships were observed in other nonvaricose neurites such as optic tract axons. Membranous organelles appear to contribute an additional obligatory volume to the cytosol that can be as much as seven times the organelles' direct volume. These observations suggest that both the cytoskeletal components, and the membrane organelles play a direct role in determining neurite shape.

It is well documented that nerve cell shape plays a direct, functional role in the development of the brain's microcircuitry (25, 27, 39) as well as in the processing of synaptic information in the adult brain. Without exception, nerve cells with different shapes seem to have different synaptic connections and presumably different functions (20, 27, 39). It is also true that as the axial geometry or caliber of a neural process changes, the local electrical properties are altered. Changes in these electrical properties can in turn lead to a modulation of synaptic efficacies (17, 24) or to changes in how such potentials are conducted along a process (29). Thus, it is safe to conclude that any intracellular mechanisms that might control neuronal form must also play an important role in controlling neuronal function.

Many studies have focused on the neuritic "cytoskeleton"—the neurotubules or microtubules (MTs),[1] neurofilaments, microfilaments, and the microtrabecular lattice (18, 48)—as the major intracellular component responsible for the control of neuritic axial geometry (16, 18, 32). Microfilaments have been implicated in growth cone movement (8, 50), and it has been suggested that MTs play a direct role in neurite outgrowth (14, 28, 49). The distribution of MTs has been studied in both dendrites and axons (9, 12, 18, 41, 47, 49, 50, 51).

In our own previous study on cat retinal ganglion cell

[1] *Abbreviations used in this paper:* MAP, microtubule-associated protein; MT, microtubule; SA, surface area; SVB, smooth vesicular bodies; SER, smooth endoplasmic reticulum; V_V, varicosity volume; V_M, mitochondrial volume; V_S, vesicular volume.

THE JOURNAL OF CELL BIOLOGY · VOLUME 98 APRIL 1984 1279–1290

dendrites (41), we noted that in addition to the conventional "cytoskeletal components," many membrane-limited organelles—mitochondria, smooth vesicular bodies (SVB), and smooth endoplasmic reticulum (SER)—also appear to make significant contributions to final neuritic form.

Using computer assisted serial electron microscopic methods (44, 45), we have further explored the possible contribution made by intracellular organelles to the control of axial geometry in a variety of neural processes including optic tract axons, sciatic axons, ganglion cell dendrites, cortical dendrites, hippocampal dendrites, and retinal cell dendrites. In the present paper, detailed results are presented on two cat retinal cell types with highly non-uniform axial shapes known as AI and AII amacrine cells and for comparative purposes we present data on a process with a more uniform axial geometry, the optic tract axon.

MATERIALS AND METHODS

Rationale For Choosing the AI and AII Cell as A Model System: While we have studied many neurites with uniform axial shapes, we selected the "non-uniform" geometry of the AI and AII amacrine cell type as a model system because it would be difficult to correlate or to quantify any fixed relationship that might exist between shape and organelles if both were uniform. A perfectly cylindrical process with constant organelle distribution and constant shape could be consistent with a variety of intracellular support mechanisms. If, however, the shape of the process were irregular and the organelles had a constant distribution, it would eliminate the organelles as a major intracellular control mechanism. Likewise, if the organelle distribution were irregular, but process shape were not irregular, we could conclude that organelles play little direct role in neurite shape control. If, however, the irregular distribution of organelles were to strongly correlate with an irregular neurite shape, it would at least suggest that organelles may play a role in shape control. Thus, since AI and AII amacrine cells have both an irregular shape and an irregular distribution of intracellular organelles, we chose these cells as

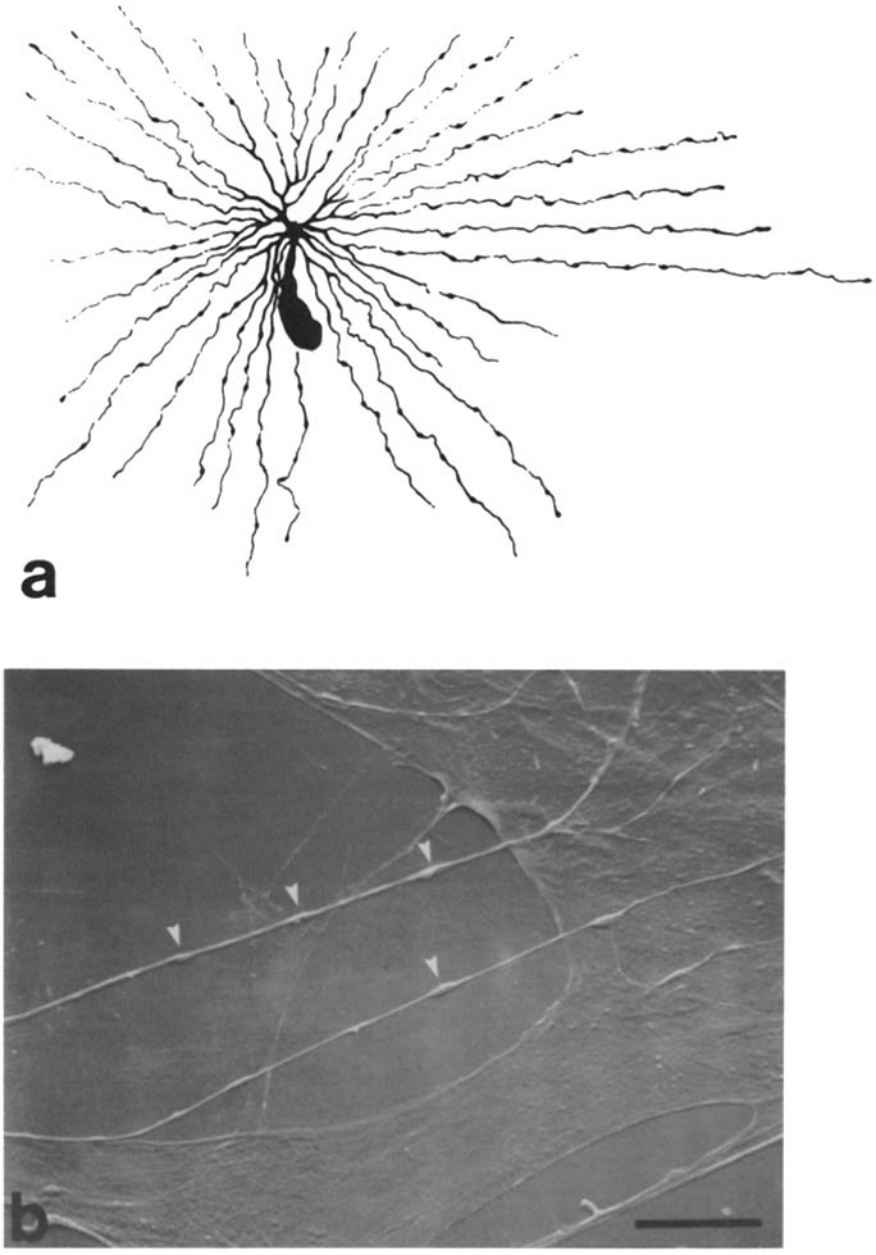

FIGURE 1 (*a*) A Golgi-impregnated amacrine cell by Cajal (10) from the Perch, *Box salpa*, showing varicose dendrites. (*b*) Scanning electron micrograph showing varicosities on neuronal processes of cat retinal tissue cultured neurons grown on fibroblasts. Bar, 10 μm.

a worst case test for the hypothesis that organelles do contribute significantly to the axial form of neurites.

Both AI and AII amacrine cells have non-uniform axial geometries consisting of long varicose like neurites. These processes have short cylindrical segments from 0.1 to 0.25 μm in diameter and 2–10 μm long that serve as interconnections between 1.0- to 2.0-μm varicose expansions (17). Such varicosities were first described by Ramon y Cajal (10) in Golgi material (Fig 1 *a*) and later by Famiglietti and Kolb (20), and Kolb (31). Similar varicosities have been observed in living, presumed amacrine cells in tissue culture as well as in other nonretinal tissue culture systems (Fig. 1 *b* and references 7, 45) as well as in other in situ neuronal systems (10, 23). Our own serial electron microscope work (17) demonstrates that each amacrine varicosity has both synaptic inputs and synaptic outputs and may act as a local input-output circuit.

Electron Microscopy: Conventional perfusion and fixation of adult cat retina were used as previously described (41). Ultrathin serial sections of selected regions of the inner plexiform layer had a pale gold interference color and were collected and placed on 0.5% Formvar-coated slot grids as per Stevens and co-workers (44, 45). Sections were stained with lead citrate and uranyl acetate (41). Three retinal series, obtained from different cats, were examined in a JEOL 100B electron microscope and analyzed as outlined below.

Scanning electron microscopy was performed upon primary cat retinal tissue cultures (Fig. 1 *b*). The culture procedure, was performed on 12-cm fetal kittens, similar to that described by Barker and Ransom (3). Processing of cells for scanning electron microscopy involved fixation with 2.5% glutaraldehyde in 0.1 M cacodylate buffer for 2 h followed by a wash with 0.1 M cacodylate buffer containing 8% sucrose (two times 5 min), postfixation with 1% osmic acid in 0.1 M cacodylate buffer for 30 min, and dehydration through 50, 70, 90, and 100% alcohols (two times 5 min each). Samples were immediately critical-point-dried, gold-coated, and viewed in a JEOL scanning electron microscope.

Analysis: Amacrine processes were serially reconstructed on a computer system as described by Stevens and Trogadis (45). All contained mitochondria were reconstructed. Only the large profiles (>150 nm) of SVB or SER were reconstructed due to the difficulty of tracing small convoluted SVB or SER profiles through serial sections. Volumes, surface areas (SA), and lengths were calculated for both varicosities and the "necks" that connected them. The delineation between varicosity and neck was arbitrarily chosen as the starting point where dendritic caliber first increased to at least twice that of the neck diameter.

Numbers of MTs within the varicosities and necks were counted and, in five amacrine processes, all of the MTs were also reconstructed. Neurofilaments were inconspicuous or absent. Volumes and SA of mitochondria and LVPs and number and SA of synaptic inputs and outputs were also calculated. All calculations assumed a section thickness of 0.1 μm. Volumes for organelles and plasma membrane were plotted as a noncumulative, section-by-section graph (see Figs. 4, 6, and 7) below the actual reconstruction to facilitate direct visual comparison.

Amacrine processes, in which all varicosities were reconstructed, were chosen randomly except for the AII varicosities taken from the cell in Fig. 2 *a*. Product-moment correlation coefficients (r), for normally distributed data, and Geometric Mean Model II linear regressions (43) were calculated for various parameters. Model II regression was used in this study since all variables were measured and therefore subject to error (43). Normality was tested using the Kolmogorov-Smirnov goodness-of-fit test (43). A nonparametric Spearman's

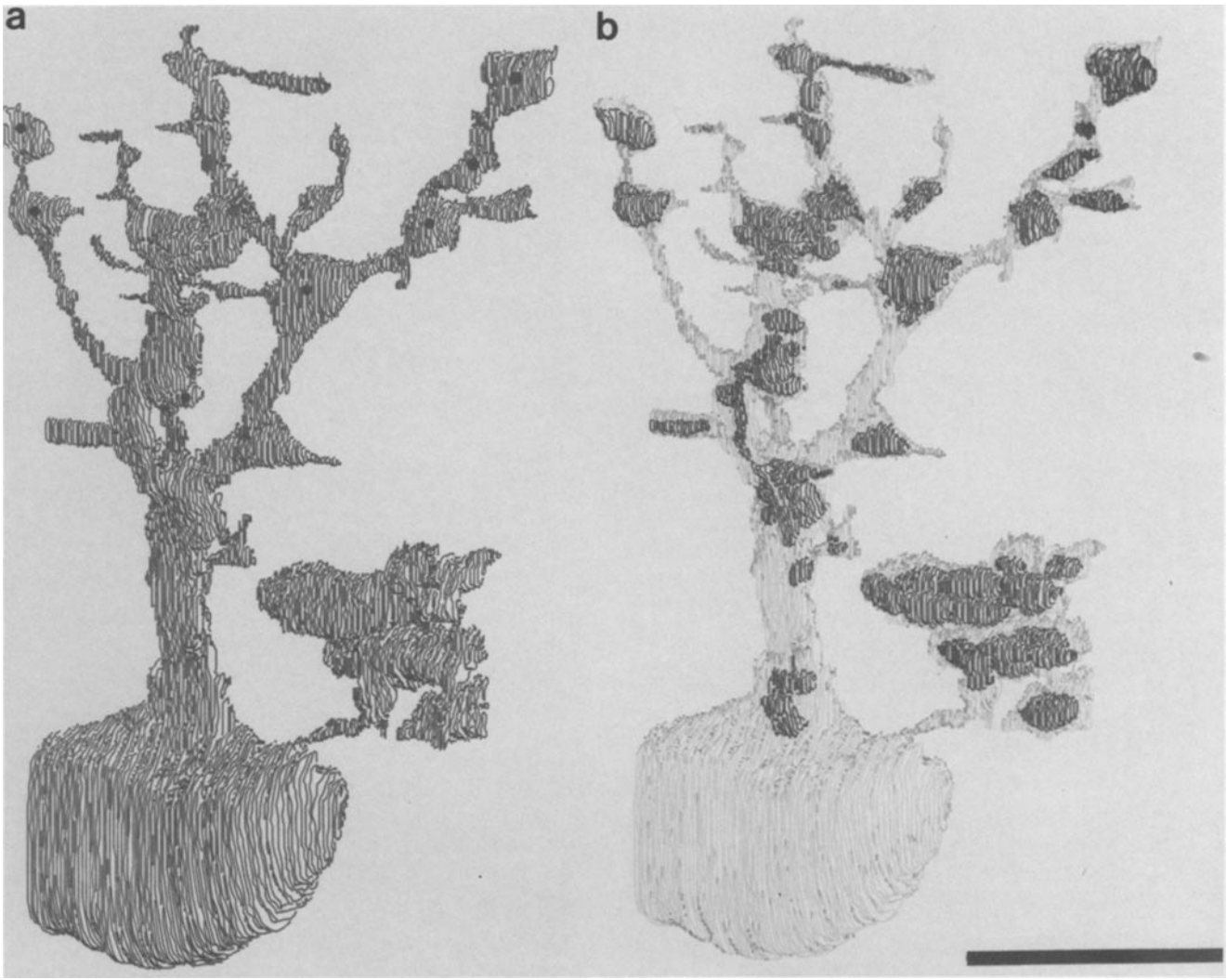

FIGURE 2 Complete reconstruction of an AII amacrine cell from adult cat retina. (*a*) Black traces represent the plasma membrane of the cell, each line indicating one section in the series. Filled circles mark the varicosities used in this study. (*b*) Grey and black traces represent the plasma membrane and mitochondria, respectively. Note that each varicosity contains at least one mitochondrion. Bar, 10 μm.

ranked correlation coefficient (r_S) was calculated for data that were skewed (AI SVB volumes and MT number, and AII data) or more closely followed a Poisson distribution (synaptic inputs and outputs). A multiple regression analysis was used to calculate the correlation coefficients and slopes, A and B, for the equation $V_V = AV_M + BV_S + k$ (Table I).

RESULTS

AI and AII Morphological Overview

The major criteria used for identifying amacrine processes were the presence of ribbon bipolar synaptic inputs, synaptic vesicles, and the characteristic varicose appearance with distinctive mitochondrial profiles (Fig. 3). Fig. 2 shows a complete reconstruction of an AII amacrine cell. The left hand figure (Fig. 2*a*) shows the outer limiting membrane of the cell as dark contours and the right hand (Fig. 2*b*) shows the outer limiting membrane as a transparent trace with intracellular organelles shown as dark profiles. Each line of the trace in both plots represents one section in the series. The dark organelle contours of Fig. 2*b* clearly show that each varicosity contains at least one mitochondrion or SVB and each organelle produces a varicosity. Consistent with our previous work on ganglion cell dendrites (41), but in contrast to retinal axons (see Figs. 9 and 10 below), these processes rarely contain continuous SER. The necks of AII amacrine dendrites, thicker than those of the AI, contain MTs, and numerous small and smooth vesicular bodies. These AII amacrine varicosities are easily distinguished from AI varicosities in single sections by their larger average size, large mitochondria with numerous, highly folded cristae, and fewer synaptic vesicles. (Fig. 3, filled stars). Varicosities of both AI and AII cells often contain SVBs (Fig. 3*b*, triangles) that are frequently associated with mitochondria.

The varicosities of the AI dendrites (see Fig. 4*a* and 6*a*; and references 17, 20, 31), containing numerous synaptic vesicles, usually one mitochondrion, SVB, and electron-lucent cytoplasm (Fig. 3, open star), were interconnected by long, thin "necks" as compared to AII necks (Fig. 2). These AI necks, often found in bundles (upper middle of Fig. 3*a*), contained little more than MTs and the rare tubule of SER. The mitochondria of AI amacrine dendrites were small, containing few cristae. Because of the long processes and their diffuse distribution, a complete reconstruction of an AI cell was not possible. Although AI amacrines have been further subdivided on the basis of synaptic connections this classifi-

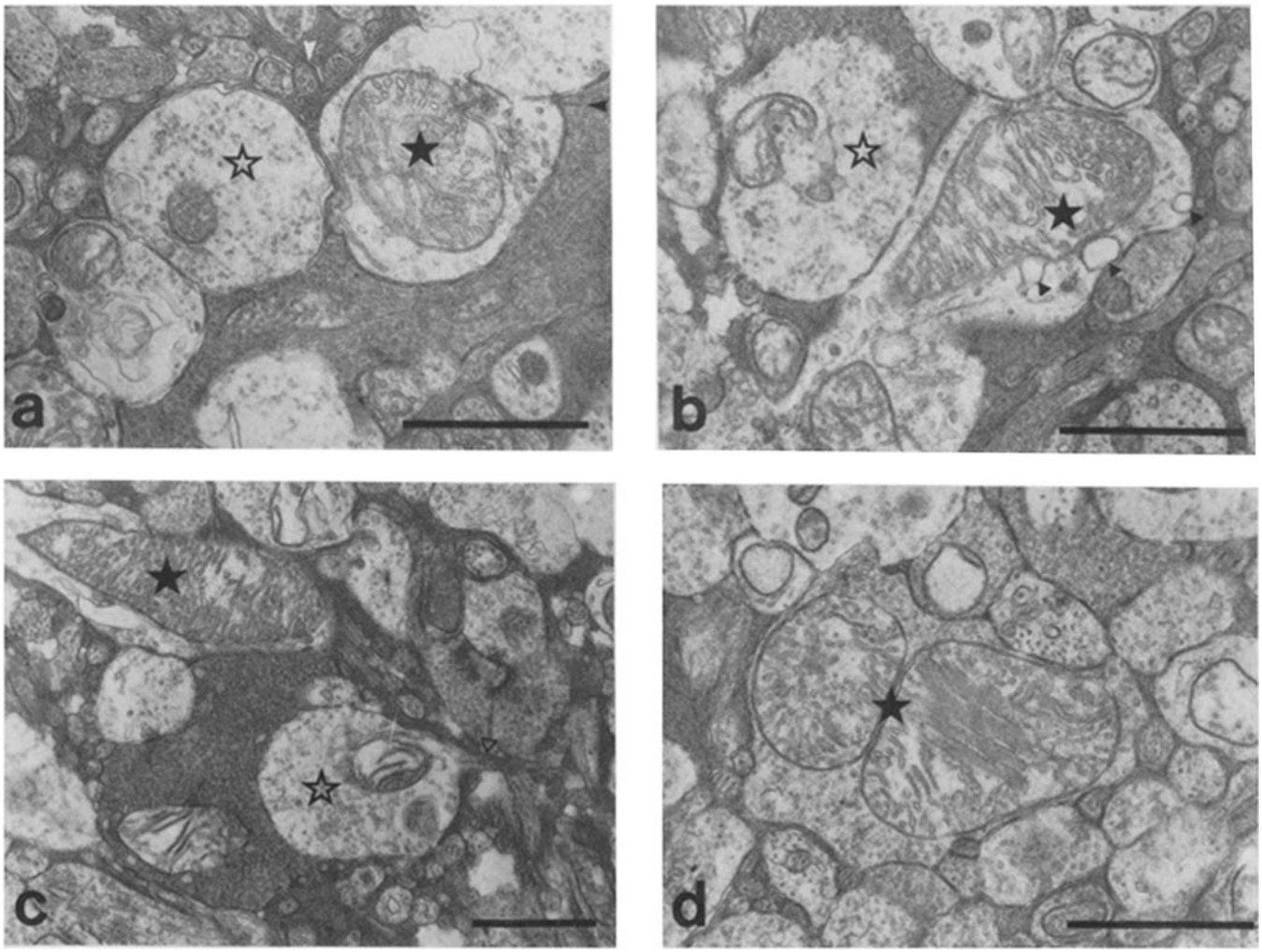

FIGURE 3 Electron micrographs of AI and AII varicosities. Filled star, AII amacrine varicosity; open star, AI amacrine varicosity. (*a*) AI and AII amacrine varicosities. Note the large, characteristic mitochondrion of the AII amacrine compared to the smaller mitochondrion of the AI amacrine dendrite. Small black arrowhead indicates a ribbon bipolar synaptic input onto the AII amacrine process. White arrowhead indicates a bundle of AI amacrine necks in cross-section. (*b*) AI and AII amacrine varicosities. (*c*) AI amacrine varicosity with neck containing two microtubules (open triangle) and AII amacrine varicosity. (*d*) AII amacrine varicosity containing two mitochondria. Bar, 1 μm.

cation was not used since the divisions are indistinguishable cytologically (31).

Correlation of MT Number with Neck and Varicosity Volume

Complete MT arrays were reconstructed in one AII amacrine process and four AI amacrines. An example of an AI reconstruction is shown in Fig. 4*a*. The black lines running the length of the reconstruction represent the MTs, the dark profiles represent the organelles and the lighter profiles the outer limiting membrane. There were no neurofilaments in any of these processes. Below, in Fig. 4*b*, is a noncumulative plot of plasma membrane volume, organelle volume (see below for details) and the effective microtubule volume. This effective microtubule volume assumes that MTs could account for some of the volume of the dendrite, consistent with our own previous work (see reference 41). To obtain this assumed MT volume, we simply assigned an arbitrary cross-sectional area (calculated from the slope of Fig. 5*b* as 0.008 μm^2 to the microtubules and treated each microtubule as a larger cylinder. The total effective volume of the MTs was then estimated as the total length of all MTs on a given section times this area. A relative comparison could then be made between this effective volume and the total process volume on the same graph.

The reconstruction and volume plots shown in Fig. 4 illustrate that MTs do not increase in number in the varicosities. In general, MTs course straight through or along one side of the varicosity in a relatively coherent bundle. Similar observations were made on all other reconstructions and recently in autonomic and in cerebral and cerebellar cortical varicosities (23).

Quantitative analysis on 22 additional reconstructed AI amacrine varicosities indicates that no correlation exists (r_S = 0.430, $P < 0.05$, $n = 22$) between MT number and varicosity mean cross-sectional area (total varicosity volume/varicosity length).

In contrast to the varicose expansions, the number of MTs do appear to be correlated with the constricted neck of the amacrine process. Fig. 5*b* is a plot of the number of MTs within each neck versus mean neck cross-sectional area (total neck volume/total neck length) for 38 AI amacrine necks reconstructed. The correlation coefficient for the relationship was $r_S = 0.780$ ($P < 0.001$) indicating a relatively strong correlation between MT number and neck caliber. (The distributions of the MT data were skewed right due to a few processes with relatively high MT numbers; thus, nonparametric correlations were used.) The reconstruction and volume analysis illustrated in Fig. 4, *a* and *b*, support this observation as well.

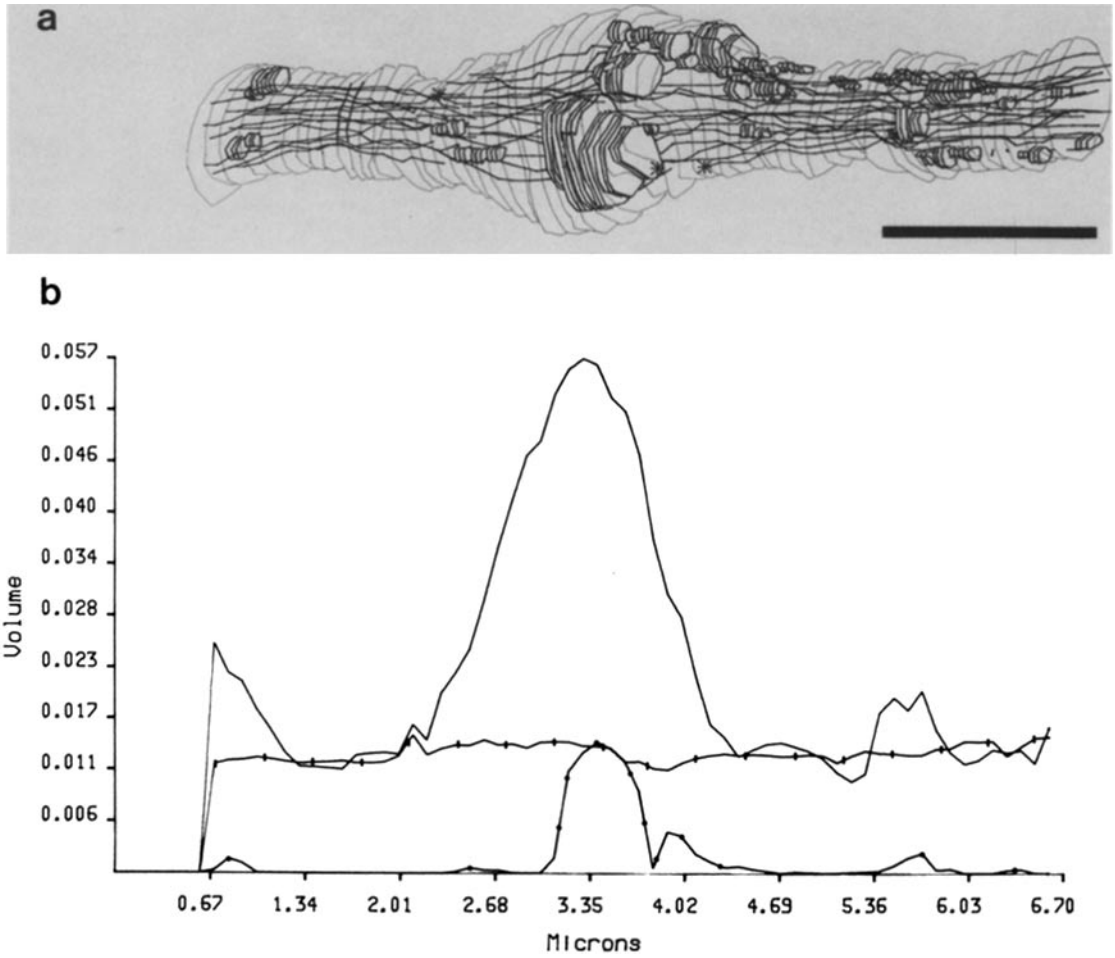

FIGURE 4 (*a*) Reconstruction of an AI amacrine dendritic segment. Grey profiles represent plasma membrane, black profiles represent SVBs (each section repeated three times), and horizontal lines indicate MTs. Bar, 1 μm. (*b*) Volume analysis of process depicted above. Volume of process (solid line), volume of SVBs (dotted line), and volume of MTs (crossed line) given in cubic micrometers (see text). Abscissa equals length of process. Series equals 64 sections. Note that for every peak in process volume there is a corresponding peak in the SVB volume.

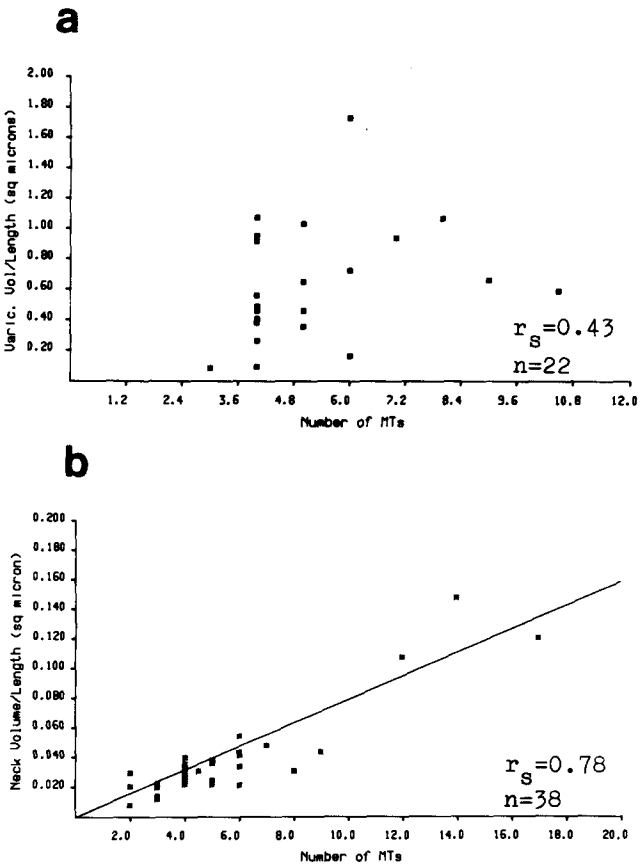

FIGURE 5 (*a*) Relationship between number of MTs in varicosity and varicosity mean cross-sectional area (varicosity volume/varicosity length) for 22 AI amacrine varicosities. Spearman's correlation coefficient (r_S) = 0.430 ($P < 0.05$). (*b*) Relationship between number of MTs in AI amacrine necks and mean neck cross-sectional area (n = 38). r_S = 0.780 ($P < 0.001$).

Varicosity Volume as a Function of Membranous Organelle Volume

While the reconstructions shown in Figs. 2 and 4 make it clear that the presence of membrane organelles is highly correlated with the presence of varicose expansions, these same recostructions also demonstrate that the organelle volume alone is not sufficient to account for the additional volume of the varicosity and that an additional factor must also contribute to the volume of the varicosity.

In Fig. 4, for example, for every increase in dendritic volume, there is a corresponding increase in the total volume of membrane organelles (dotted line). However, the total process volume shows a large additional volume beyond that of the organelles. This can also be seen in Figs. 6 and 7.

These data were further quantitatively analyzed to see if the excess volume might in some manner be related to the organelle volume or some other factor. The total plasma membrane volume was plotted along with the internal membrane organelle volume for 60 AI and AII amacrine varicosities in a fashion similar to that seen in Figs. 4, 6, and 7. The total varicosity volume was estimated by integrating between the two inflection points on these noncumulative volume graphs, and compared to the total organelle volume within that same region.

A plot of the total organelle volume versus the total varicosity volume was made for all 60 of these measurements and is shown in Fig. 8. The stars and squares represent AI and AII amacrine varicosities respectively identified using the independent criterion described above. This figure shows two totally unexpected results. First, the correlation coefficient for membrane organelle volume to varicosity volume was very high (AI $r_S = 0.927$, $P < 0.001$, $n = 32$, and AII $r_S = 0.987$, $P < 0.001$, $n = 28$) and suggests a direct, linear relationship between the volume of membrane-limited organelles and varicosity volume. Second, the slopes for the AI and AII amacrine cell types are different. Using the Geometric Mean Model II regression, the slopes were calculated as 6.97 for AI amacrine dendrites and 1.80 for the AII amacrine varicosities.

These differences between organelle volume and varicosity volume are also clear in Figs. 4, 6, and 7. Fig. 7*b* shows that the volume of mitochondria and SVBs in the AII amacrine much more closely approximates the volume of the varicosity as compared to the AI amacrine process seen in Figs. 4 and 6. Finally, the electron micrographs of these two cell types (Fig. 3) also reveal a marked difference in the area of the varicosity occupied by the mitochondria.

Other Morphometric Correlations

The relationships between varicosity SA to organelle SA, varicosity SA to organelle volume, and varicosity volume to organelle SA, were also tested. All comparisons showed significant correlations although less than the varicosity volume to organelle volume relationship (Table I).

Since varicosities are the major sites for synaptic communication in amacrine processes (17, 31), varicosity size could be related to synaptic inputs and/or outputs as others have suggested for motor nerve terminals (2). Varicosity volume was, therefore, correlated with number and SA of synaptic inputs, outputs, or total contacts and the correlation coefficients are listed in Table II.

The AI amacrine varicosity volume correlates best with the total number of contacts or synaptic outputs; the AII volumes correlate best with total contacts or synaptic inputs (Table II). The r^2 values for total synaptic contacts range from 0.512 to 0.686 indicating that up to 69% of the variance in varicosity volume can be explained by SA or number of synaptic contacts.

While these correlations are significant, 4 of 25 AI amacrine varicosities and 4 of 20 AII amacrine varicosities had no detectable synapses. Additionally, one AI and five AII amacrine necks had one and nine synaptic inputs, respectively, suggesting a nonessential relationship between synaptic contacts and varicosities.

Correlations between Organelles Contained in a Single Varicosity

Single AI varicosities often contained several organelles. (e.g., Fig. 4). Since in most cases these organelles consisted of a single mitochondrion and several vesicular bodies, the two fractions (mitochondria and SVB) found in single varicosities could be correlated.

The correlation coefficient for total mitochondrial versus the total vesicular volume fractions was $r_S = 0.534$ ($P < 0.01$) for 32 AI amacrine varicosities; the mitochondrial SA to vesicular SA correlation was $r_S = 0.536$ ($P < 0.01$). Although significant, the correlations were far lower than expected given the very high correlation of $r = 0.927$ between total organelle volume and varicosity volume.

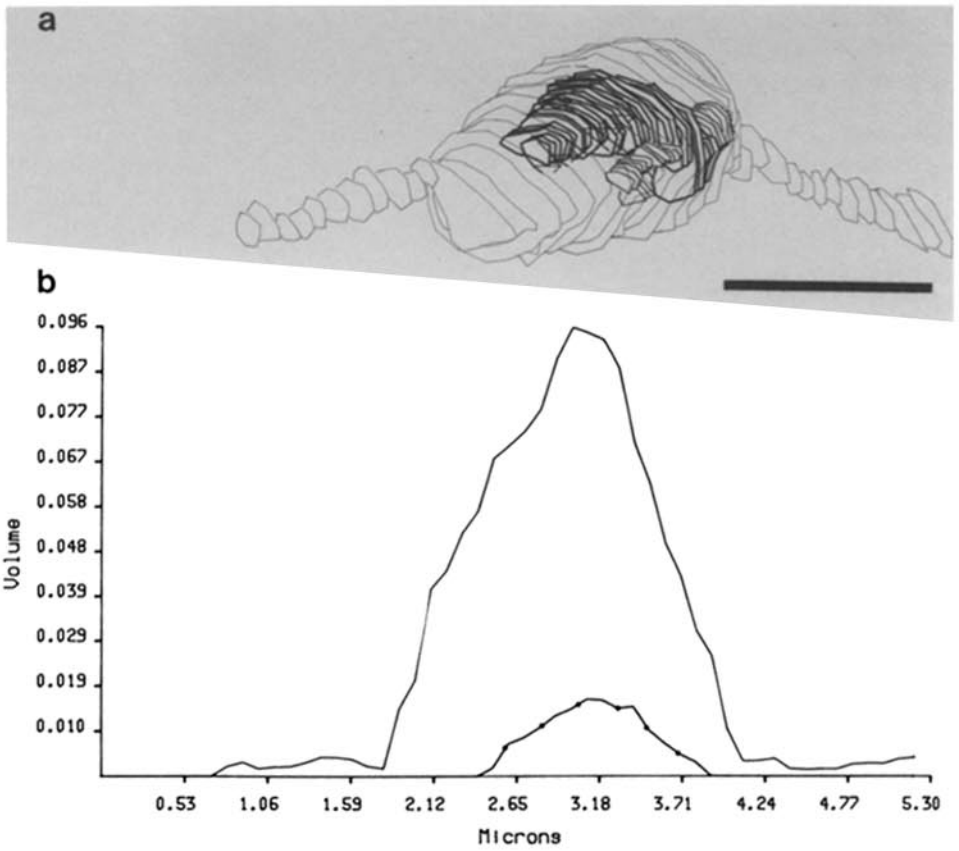

FIGURE 6 (*a*) Reconstruction of an AI amacrine dendritic segment. Grey profiles represent plasma membrane, thick black traces represent mitochondria, and thin black traces indicate SVBs. Organelle traces are repeated three times. Arrows indicate synaptic input. Bar, 1 μm. Note large varicosity with very thin necks. (*b*) Volume analysis of AI amacrine dendrite depicted above. Volume of process (solid line) and summed volume of organelles (dotted line) in cubic micrometers. Abscissa equals length of process. Series equals 59 sections.

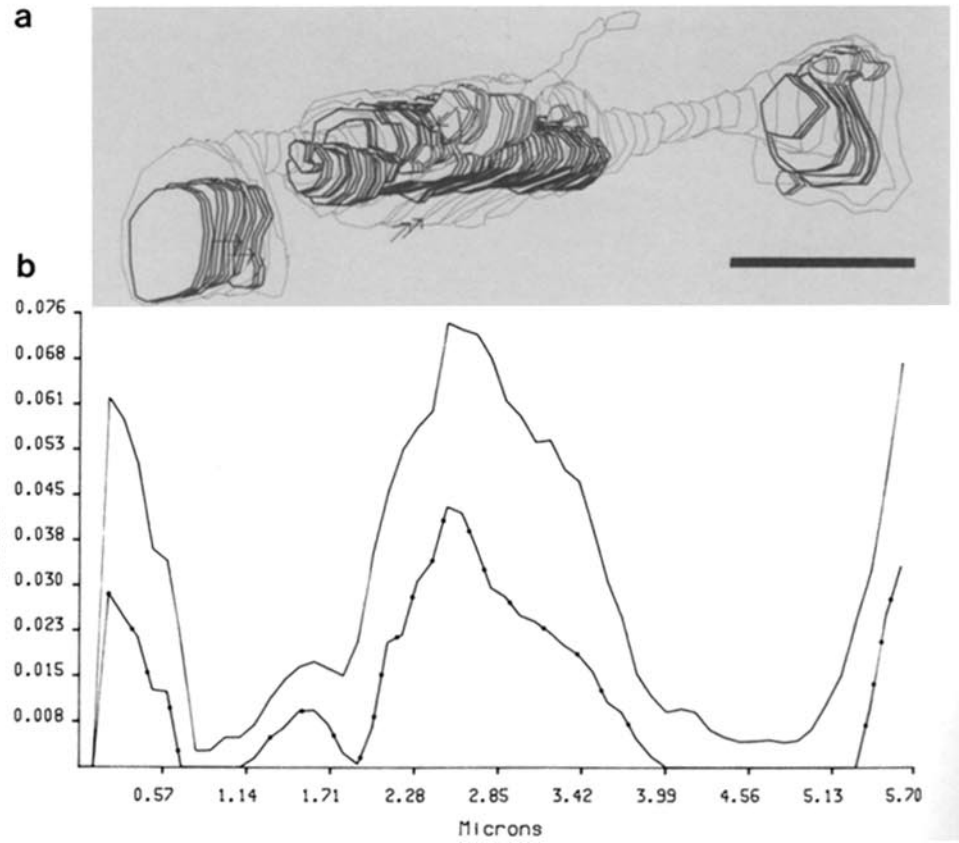

FIGURE 7 (*a*) Reconstruction of an AII amacrine dendritic segment. Same as Fig. 6*a*. (*b*) Volume analysis of AII amacrine dendrite shown above. Same as Fig. 6*b*.

If both the mitochondria and SVBs were influencing the size of varicosities, it would also seem reasonable that they might have their own independent, individual volume ratios which, when added may create the ratios seen in Fig. 8. In other words, since the slopes for the total organelle contribution were different for AI and AII amacrine cells, it is also

possible that the slopes for SVBs and mitochondria, might be different within a single cell type.

The two equations below, in which V_V is the varicosity volume, V_M the mitochondrial volume, and V_S the vesicular volume (SVBs, MVBs, lysosomes), represent possible relationships between varicosity volume and organelle volume:

$$V_V = a\,(V_M + V_S) + k \qquad \text{or} \qquad (1)$$

$$V_V = AV_M + BV_S + k, \qquad (2)$$

where a, A, and B are slopes and k is the intercept. Eq. 1 can also be written $V_V = aV_M + aV_S + k$ and represents the case in which V_M and V_S influence V_V with identical slopes. Table III lists correlation coefficients and constants for the two cell types.

The correlation coefficient for AI V_V vs. V_M alone (AV_M) was r = 0.869 ($P < 0.001$, $n = 32$) and could explain 75.6% of the variation in V_V. When included in the AI amacrine regression analyses, the V_S's improved the correlations. The coefficient for the relationship, $a\,(V_M + V_S)$, was $r = 0.927$ ($P < 0.001$, $n = 32$), explaining 85.9% of the variance in V_V. The same volumes, when analyzed for the relationship, $AV_M + BV_S$, using multiple regression analysis, gave a correlation coefficient of $r = 0.936$, explaining 87.5% of the variance. Although the difference between the r^2 values is small, Eq. 2 can explain more of the variance in V_V than Eq. 1 and, therefore, may more closely approximate the true relationship. The slopes for AI V_M (mitochondria) and V_S (SVBs) were $A = 5.60$ and $B = 9.67$, respectively.

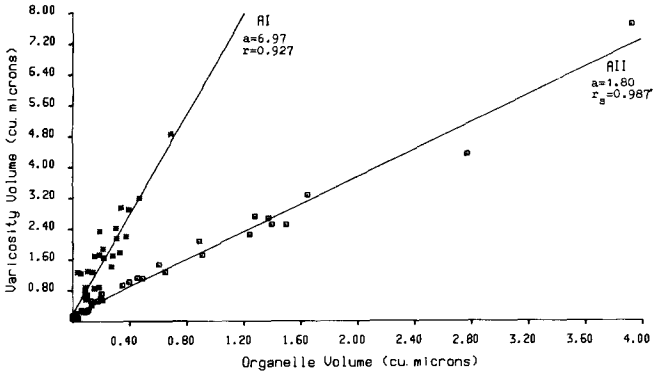

FIGURE 8 Relationship between the summed volume of mitochondria and/or SVBs in a varicosity and varicosity volume for AI and AII amacrine varicosities. For AI amacrine varicosities (stars), $r = 0.927$ ($P < 0.001$, n = 32) and for AII amacrine varicosities (squares), $r_S = 0.987$ ($P < 0.001$, $n = 28$).

These results indicate that the volumes correlated with the organelles appear to be independent for SVBs and the mitochondria even within the same cell type, as well as in different cell types.

Analysis of Uniform Neurites

As stated in the introduction, analyses have been carried out similar to that described above on a variety of uniform dendrites, ganglion cell axons, and peripheral sciatic axons. Although detailed quantitative analysis was not carried out since it is not possible to compartmentalize the plasma membrane volumes, correlations between the organelle fraction, MT fraction, and total process volume similar to that seen in Figs. 4, 6, and 7, were possible.

We illustrate these results in Figs. 9 and 10. The top Fig. 9 is an outside view of a short segment serial electron microscopic reconstruction of an optic tract axon. The lower portion of Fig. 9 illustrates the contained organelles. It is interesting that the SER appear to be continuous in this axon material as compared to the AI and AII reconstructions. Fig. 10 is a volume plot of the plasma membrane (upper portion graph) and the total organelle volume (lower plot). Using cross-correlogram methods one could assign a slope to the organelle fraction and predict the average variations in total process volume along its length. Similar relationships have been observed in all nonmyelinated axonal reconstructions to date (over 50) and in all dendritic reconstructions (over 45)

TABLE II
Correlation Coefficients

Varicosity volume		Synaptic contacts		
Cell type		Inputs	Outputs	Total
AI ($n = 25$)	No.	$r_S = 0.634$ $P < 0.001$	$r_S = 0.754$ $P < 0.001$	$r = 0.716$ $P < 0.001$
	SA	$r_S = 0.459$ $P < 0.02$	$r_S = 0.726$ $P < 0.001$	$r = 0.724$ $P < 0.001$
AII ($n = 20$)	No.	$r = 0.844$ $P < 0.001$	$r_S = 0.440$ NS	$r = 0.828$ $P < 0.001$
	SA	$r = 0.792$ $P < 0.001$	$r_S = 0.399$ NS	$r = 0.792$ $P < 0.001$

Correlation coefficients for the relationship between varicosity volume and number or SA of synaptic inputs, outputs, or total contacts for AI and AII amacrine varicosities. *NS*, not significant.

TABLE I
List of Correlation Coefficients

	AI amacrine dendrites		AII amacrine dendrites	
	Organelle volume	Organelle surface area	Organelle volume	Organelle surface area
Varicosity volume	$r = 0.927$ Slope = 6.97 $P < 0.001$	$r = 0.918$ Slope = 0.71 $P < 0.001$	$r_S = 0.987$ Slope = 1.80 $P < 0.001$	$r_S = 0.974$ Slope = 0.44 $P < 0.001$
Varicosity surface area	$r = 0.888$ Slope = 22.17 $P < 0.001$	$r = 0.911$ Slope = 2.27 $P < 0.001$	$r_S = 0.973$ Slope = 5.08 $P < 0.001$	$r_S = 0.976$ Slope = 1.23 $P < 0.001$

List of correlation coefficients (parametric for AI amacrine varicosities; Spearman's for AII amacrine varicosities; see Method), comparing various relationships between amacrine organelle volume or surface area and amacrine varicosity volume or surface area. Sample sizes of 28 varicosites for AI amacrines and 32 varicosities for AII amacrines.

TABLE III

Correlation coefficients

Cell type	Equation tested	Slope	k	r	r^2
AI	$V_V = AV_M + k$	$A = 7.47$	0.316	0.869*	0.756
AI	$V_V = a\,(V_M + V_S) + k$	$a = 6.97$	0.207	0.927*	0.859
AI	$V_V = AM + BVS + k$	$A = 5.60$ $B = 9.67$	0.203	0.936*‡	0.875
AII	$V_V = a(V_M + V_S) + k$	$a = 1.80$	0.187	0.987*‖	—
AII	$V_V = AV_M + BV_S + k$	Not performed			

Correlation coefficients (r) and constants for the varicosity volume to membranous organelle volume relationship in AI ($n = 32$) and AII ($n = 28$) amacrine dendrites.

* $P < 0.001$.

‡ Multiple regression analysis used.

‖ Spearman's coefficient of rank correlation (42).

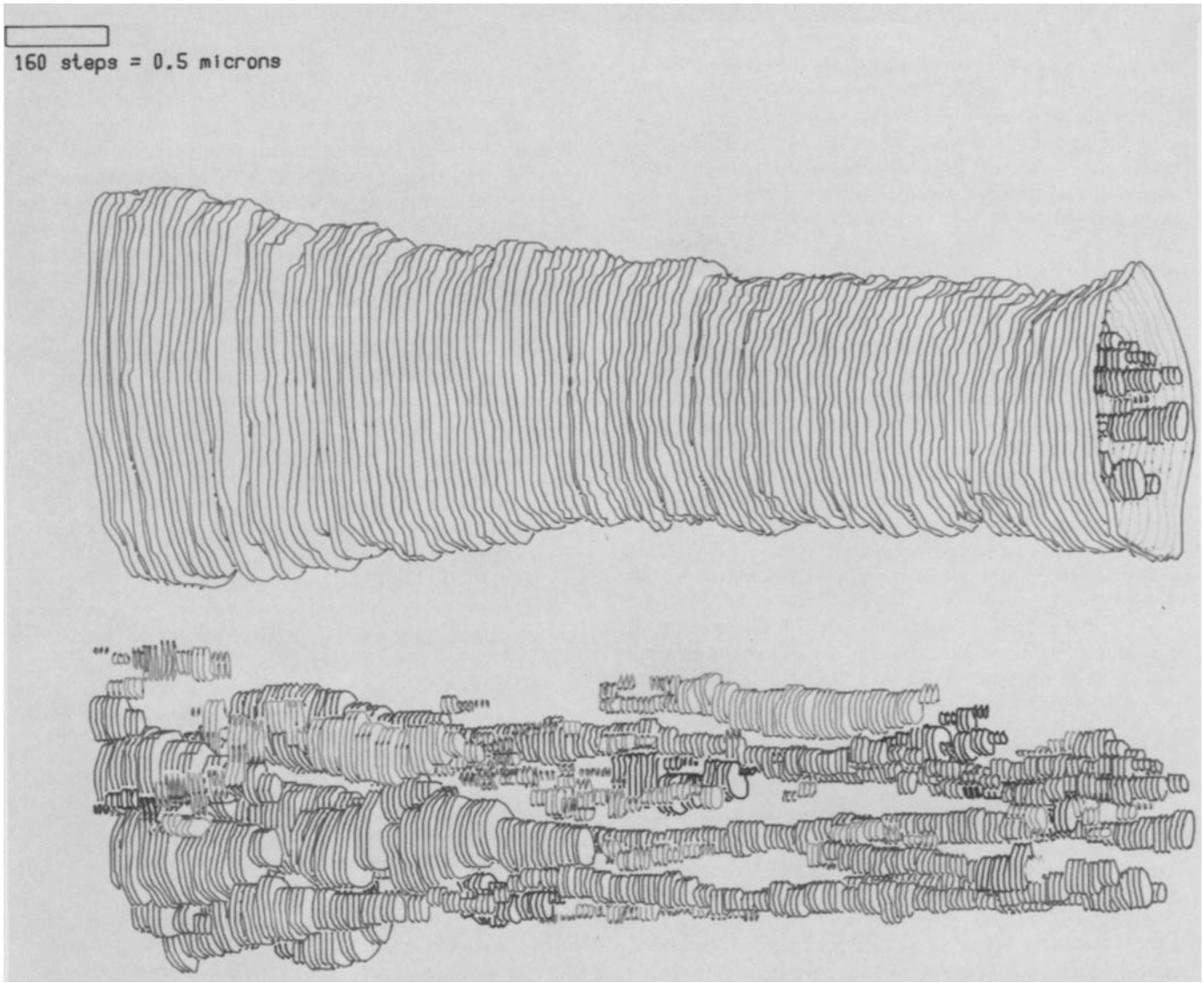

FIGURE 9 Reconstruction of a short optic tract segment. The top portion of the figure is an external view of the axon. The lower view are the contained organelles.

examined to date. A complete report of the axonal data will be presented in a future paper.

DISCUSSION

In a previous paper (41) we suggested that the microtubular array served as a major determinant of axial shape in cat retinal ganglion cell dendrites. It was also clear in that study that intracellular organelles must make some direct contribution to dendritic volume—minimally equal to their own volume. We noted, however, an additional volume beyond that directly contributed by both the organelles and the MTs that could not be easily explained. Since these dendrites had

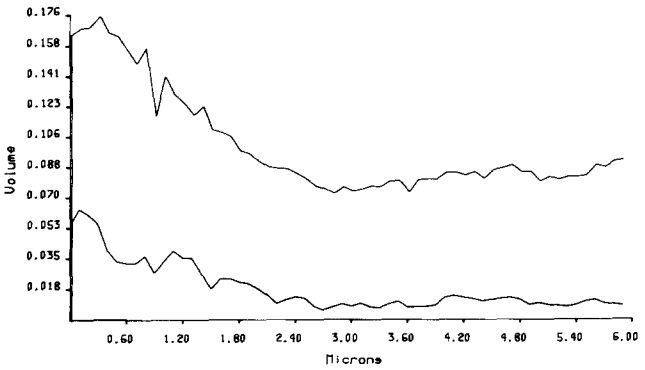

FIGURE 10 Plot of volumes from the optic tract axon shown in Fig. 9. Upper plot is the plasma membrane, and the lower plot are the contained organelles.

reasonably uniform axial geometries and uniform intracellular distributions of organelles it was not possible to systematically study the source of this excess volume.

In the present study we have focused on AI and AII amacrine cells because they have non-uniform axial geometries as well as non-uniform distributions of organelles. Their neurites consist of 1–3-μm varicose expansions connected by much narrower 2–10-μm long cylindrical necks. Consistent with our earlier observations on ganglion cell dendrites, we found that MT density correlates with the diameter of the organelle free regions of both AI and AII neurites (i.e., the connecting neck). Without exception, we found that each organelle or group of organelles corresponded to a varicosity and that each varicosity contained organelles. Finally, we also found that the varicosity always contained an excess volume beyond that of the organelles. Moreover, the MTs did not increase in number within the varicosity, nor did they follow the plasma membrane as might be expected if they formed a varicose frame or ribbing similar to the marginal band of platelets and nucleated erythrocytes (16, 22).

Through three dimensional morphometric analysis we discovered that this excess volume was linearly related to the volume of the contained organelles. Additionally, slopes of the volume functions were different for different organelles (e.g., SVB vs. mitochondria) in the same cell or in different cells. The interpretation and significance of these observations is outlined below.

MT Cytoskeleton as a Correlate of Neck Volume

The strong correlation between MT number and neck caliber (r_S = 0.780, $P < 0.001$, Fig. 5) suggests a direct relationship. In his study of MTs in cells of *Juniperus* root tip, Porter (37) first revealed an electron-lucent region surrounding each MT, suggesting there was more to the MT than could be seen by conventional electron microscopy stains. Similar conclusions and observations have been made made by Behnke (4, 5) and our own data from ganglion cells suggested that each MT may be modeled as a large, independent, cylindrical tube, with a total diameter beyond that seen in conventional micrographs (41). We suggested that area surrounding the MTs could be created by microtubule-associated proteins (MAPs) inserted into and protruding from the surface of the polymer, creating a "bristle effect" (30, 46, 52) or surrounding cylinder.

Many authors have reported filaments extending from MTs and bridges between MTs (e.g., 40). Dentler et al. (15) showed that purified brain tubulin, polymerized in the presence of high molecular weight MAPs produced MTs with filaments jutting from their surfaces. Similar results were obtained by Kim et al. (30), Herzog and Weber (26), and Zingsheim et al. (52) using MAP2; the presence of MAPs on each MT kept the tubules spaced a regular distance apart. It was suggested (52) that the presence of MAPs in brain tissue may act in a similar manner in situ. Thus each MT, encased in a coating of MAPs, may significantly increase the neurite's volume (41) and, in this way, contribute directly to the caliber of neuronal processes.

Organelle Volume as a Correlate of Varicosity Volume

Friede and Martinez (21, 34) found that the greater the accumulating density of mitochondria in transected rat sciatic axons, the greater was the axonal swelling. Although axonal swelling was well correlated with the collected organelle density, the total volume of the organelles could not wholly account for the total increase in axonal volume observed (34). Using single section electron microscopic morphometry, Alnaes and Rahamimoff (2) also report a loose relationship between the volume of motor terminals and mitochondrial volume. Our own serial electron microscopic data presented above lead us to make a number of conclusions concerning organelle contributions to neuritic volume beyond these original observations.

Of all relationships tested, varicosity volume and organelle volume had an unusually significant correlation coefficient of 0.987. (Table I). Moreover, the different volume slopes for organelles in independently identified AI and AII amacrine cells suggests that cell type can influence the observed organelle-varicosity volume relationships differentially. (The AI ratio was 1:6.97, the AII ratio was 1:1.80). Additionally, the multiple regression analysis on AI cells showed that mitochondrial and vesicular volumes were related to varicosity volume by different slopes (Table III). This suggests that different organelles within the same cell type influence varicosity volumes differentially. This is reassuring since it is unlikely that the different organelles could influence varicosity volume by exactly the same factor. Equal slopes might have indicated that the results were artifactual or that varicosity volume determined the volumes of mitochondria and vesicular organelles.

Does Varicosity Volume Determine Organelle Volume or Does Organelle Volume Determine Varicosity Volume?

The correlations and relationships described above are consistent with the possibility that the organelle actually controls and creates the observed excess volume, and that this volume could play a significant role in neuritic shape control. However, these data do not eliminate other possibilities such as direct control of SVB and mitochondrial volume by the varicosity itself (e.g., active pumps in the plasma membrane) or by the some other secondary mechanism.

If the varicosity were controlling the organelle volume we might expect a high correlation between the volumes of the SVBs and mitochondria contained within a single varicosity. All organelles in a large varicosity would also be large or at least correlated. If, on the other hand the organelles were

responsible for the varicosity volume we might expect a very low correlation between organelles contained within a single varicosity. The multiple regression analysis demonstrated that shared mitochondrial and vesicular volumes within the same varicosity were poorly correlated ($r_s = 0.536$, $P < 0.01$, $n = 32$). Thus, this poor correlation between organelles contained in a single varicosity supports the conclusion that the organelles determine varicosity volume not vice versa.

Furthermore, if varicosity volume did determine membrane organelle volume, the question would remain: what determines the excess volume found in the varicosity? Although a correlation does exist between number of synaptic contacts or surface area of total synaptic contacts and varicosity volume, we observe varicosities with no detectable synapses and on on occasion necks were found with synaptic contacts. Thus synaptic contacts cannot be the major determinant of varicosity size. The possibility that surrounding cells, impinging on the dendrite, create the varicosities is unlikely since varicosities also exist in tissue culture (Fig. 1 *b*; see reference 42) and are seen to move in time lapse photography as described by Breuer et al. (7).

These observations lead us to conclude that the excess volume contained within each varicosity is actually an obligatory volume associated with the contained organelles. Given the different obligatory volume for AI and AII cell organelles it seems possible that each cell type may actually use this obligatory volume to differentially control its final form and thus control its final function. Stated in another way, it is also possible that the AI and AII amacrine cells have different axial silhouettes because they have organelles with different obligatory volumes.

Possible Cellular Mechanisms for the Obligatory Volume

If organelle volume determines varicosity volume, the mechanism is likely to be fairly rapid since varicosities (or organelles) travel along neurites in tissue culture at rates of 0.17–0.47 μm/s (7; and personal observation). A physical reaction, such as local osmotic swelling, caused by the extrusion of an ion or molecule (solute) by the organelle, might explain the extremely high correlations between organelle volume and varicosity volume.

Release or leakage of a solute from the organelle could induce localized movement of extracellular water into the process to preserve osmotic/ionic equilibrium similar to that seen during the chloride shift in erythrocytes. This obligatory osmotic volume, might be controlled by a variety of factors such as the total size of the solute source within the organelle, the rate of an active solute pump associated with the organelle, the reverse leakage rate from the organelle to the cytoplasm as well as the cytoplasm's ability to buffer the solute. Any or all of these factors could contribute to the different obligatory volumes encountered in the different organelle types and the two cell types.

Since mitochondria and SVBs are both known to sequester Ca^{++} (1, 2, 6, 11, 19, 33, 35, 36, 38), both have been implicated in the control of intracellular CA^{++} during neurotransmitter release, and may even release Ca^{++} during depolarization (2, 38), Ca^{++} is a plausible candidate. Its movement is effectively controlled by calcium-binding proteins and calcium pumps (11, 13, 36). It is also possible that, apart from an osmotic effect, local changes in ion (e.g., Ca^{++}) concentration could induce changes in the cross-linking density of the microtrabecular lattice (48) allowing greater cytosol volume between structural elements. The mechanism is open to speculation, and will require further research.

Obligatory Volume as a General Principle

We have observed similar obligatory volumes in several other systems including dendrites from retinal, cortical, and hippocampal material, and finally, in both central and peripheral axons. Figs. 9 and 10 illustrate the relationship between organelle volume and total process volume in a optic tract axon. These axonal results are of particular interest since the position, size, and number of organelles might then play a significant role in the determination of axon conduction velocity by affecting both the caliber of a process as well as the distribution of surface area along its length. It will be important, however, in future studies to quantify these obligatory volumes in processes with uniform axial geometries using cross-correlation methods and very long series.

Summary and Conclusions

Considering the tremendous diversity of neuronal form, it is likely that there are many different and unique mechanisms that might contribute to the final axial shape of an arbitrary neurite. However, the factors described in the present study seem sufficient to account for much of the axial geometry of AI and AII amacrine cells, retinal ganglion dendrites, and optic tract axons. We have summarized these factors in Fig. 11. First, it is clear from the work of many others (4, 5, 15, 26, 30, 37, 40, 52), as well as our own work (41), that as the number of microtubules changes the neurite caliber also change: the fewer microtubules present, the smaller the caliber of the process. Second, the size, molecular weight, and chemical properties of the MAPs coating the microtubules might also be varied, thereby changing the effective radius of each microtubule (15, 26, 30, 37, 41, 46, 52). The presence and number of neurofilaments (not considered in this study) found in larger neurites are also involved in determining axial shape. Finally, as we have demonstrated in the present study, the size and location of membrane organelles may also play a direct role in determining axial shape. The ratio with which organelle volume is related to the excess volume surrounding each organelle—the obligatory volume—may be altered to change local geometry.

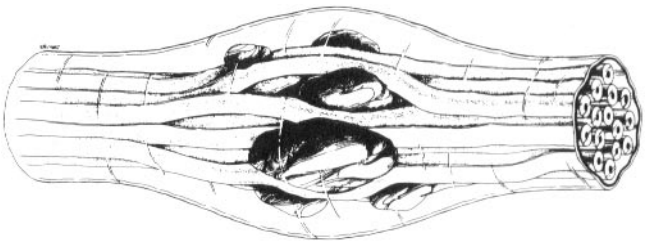

FIGURE 11 Summary figure of factors that might control the axial shape of a neurite. The microtubule number can be increased and/or decreased, and the MAPs (larger circles around the microtubules) could change in size and distribution. Finally, the obligatory volumes associated with the organelles appear to be changeable, and the distribution and location of the organelles can be altered via transport systems contained within the neurite.

We thank Judy Trogadis for her technical support and B. McGuire for her help in collecting the data for Fig. 2.

This work was supported by grants from the Canadian Medical Research Council, and the Kroc Foundation.

Received for publication 16 August 1983, and in revised form 12 December 1983.

REFERENCES

1. Akerman, K. E. O., and D. G. Nicholls. 1981. Intrasynaptosomal compartmentalization of calcium during depolarization-induced calcium uptake across the plasma membrane. *Biochim. Biophys. Acta.* 645:41–48.
2. Alnaes, E., and R. Rahamimoff. 1975. On the role of mitochondria in transmitter release from motor nerve terminals. *J. Physiol. (Lond.).* 248:285–306.
3. Barker, J. L., and B. R. Ransom. 1978. Amino acid pharmacology of mammalian central neurons grown in tissue culture. *J. Physiol. (Lond.).* 280:331–354.
4. Behnke, O. 1975. An outer component of microtubules. *Nature (Lond.).* 257:709–710.
5. Behnke, O. 1975. Studies on isolated microtubules. Evidence for a clear space component. *Cytobiologie.* 11:366–381.
6. Blaustein, M. P., R. W. Ratzlaff, N. C. Kendrick, and E. S. Schweitzer. 1978. Calcium buffering in presynaptic nerve terminals. I. Evidence for involvement of a nonmitochondrial ATP-dependent sequestration mechanism. *J. Gen. Physiol.* 72:15–41.
7. Breuer, A. C., C. N. Christian, M. Henkart, and P. G. Nelson. 1975. Computer analysis of organelle translocation in primary neuronal cultures and continuous cell lines. *J. Cell Biol.* 65:562–576.
8. Bray, D., and M. B. Bunge. 1973. The growth cone in neurite extension. *Ciba Found. Symp.* 14:195–209.
9. Bray, D., and M. B. Bunge. 1981. Serial analysis of microtubules in cultured rat sensory axons. *J. Neurocytol.* 10:589–605.
10. Cajal, S. Ramon y. 1972. The Structure of the Retina. (Translated by S. A. Thorpe and M. Glickstein.) Charles C Thomas, Springfield, IL.
11. Carafoli, E. 1981. The uptake and release of calcium by mitochondria. *In* Mitochondria and Microsomes. C. P. Lee, G. Schatz, and G. Dallner, editors. Addison-Wesley Publishing Co., MA. pp. 357–374.
12. Chalfie, M., and J. Thomson. 1979. Organization of neuronal microtubules in the nematode *Caenorhabditis elegans. J. Cell Biol.* 82:278–289.
13. Cheung, W. Y. 1979. Calmodulin plays a pivotal role in cellular regulation. *Science (Wash. DC).* 207:19–27.
14. Daniels, M. P. 1972. Colchicine inhibition of nerve fiber formation in vitro. *J. Cell Biol.* 53:164–174.
15. Dentler, W. L., S. Granett, and J. L. Rosenbaum. 1975. Ultrastructural localization of the high molecular weight proteins associated with in vitro assembled brain microtubules. *J. Cell Biol.* 65:237–241.
16. Dustin, P. 1978. Microtubules. Springer-Verlag, Berlin.
17. Ellias, S. A., and J. K. Stevens. 1980. The dendritic varicosity: a mechanism for electrically isolating the dendrites of cat retinal amacrine cells? *Brain Res.* 196:365–372.
18. Ellisman, M. H., and K. R. Porter. 1980. Microtabecular structure of the axoplasmic matrix: visualization of cross-linking structures and their distribution. *J. Cell Biol.* 87:464–479.
19. Erulkar, S. D., and A. Fine. 1979. Calcium in the nervous system. *Rev. Neurosci.* 4:180–232.
20. Famiglietti, E. W., and H. Kolb. 1979. A bistratified amacrine cell and synaptic circuitry in the inner plexiform layer of the retina. *Brain Res.* 84:293–300.
21. Friede, R. L., and A. J. Martinez. 1970. Analysis of the process of sheath expansion in swollen nerve fibers. *Brain Res.* 19:165–182.
22. Goniakowska-Witalinska, L., and W. Witalinska. 1970. Evidence for a correlation between the number of marginal band microtubules and the size of the vertebrate erythrocytes. *J. Cell Sci.* 22:397–402.
23. Gordon-Weeks, P. R., R. D. Burgoyne, and E. G. Gray. 1982. Presynaptic microtubules: organization and assembly/disassembly. *Neuroscience.* 7(3):739–749.
24. Graubard, K., and W. H. Calvin. 1979. Presynaptic dendrites: implications of spikeless synaptic transmission and dendritic geometry. *In* The Neurosciences Fourth Study Program. F. O. Schmitt and F G. Worden, editors. The MIT Press, Cambridge, MA. pp. 317–331.
25. Grinnell, A. D. 1979. Specificity of neurons and their interconnections. *In* Handbook of Physiology: The Nervous System. J. M. Brookhart and V. B. Mountcastle, editors. American Physiological Society, Bethesda, MD. pp. 803–853.
26. Herzog, W., and K. Weber. 1978. Fractionation of brain microtubule-associated proteins. *Eur. J. Biochem.* 92:1–8.
27. Hillman, D. E 1979. Neuronal shape parameters and substructures as a basis of neuronal form. *In* The Neurosciences Fourth Study Program. F. O. Schmitt and F. O. Worden, editors. The MIT Press, Cambridge, MA. pp. 477–498.
28. Hoffman, H. 1952. Acceleration and retardation of the process of axon-sprouting in partially denervated muscles. *Aust. J. Exp. Biol. Med. Sci.* 30:541–550.
29. Katz, B. 1966. Nerve, Muscle, and Synapse. McGraw-Hill, New York.
30. Kim, H., L. I. Binder, and J. L. Rosenbaum. 1979. The periodic association of MAP2 with brain microtubules in vitro. *J. Cell. Biol.* 80:266–276.
31. Kolb, H. 1979. The inner plexiform layer of the cat: electron microscopic observations. *J. Neurocytol.* 8:295–329.
32. Lasek, R. J. 1981. The dynamic ordering of neuronal cytoskeletons. *Neurosci. Res. Prog. Bull.* 19(1):7–32.
33. Lehninger, A. L. 1965. The Mitochondrion: Molecular Basis of Structure and Function. Benjamin, Menlo Park, CA.
34. Martinez, A. J., and R. L. Friede. 1970. Accumulation of axoplasmic organelles in swollen nerve fibers. *Brain Res.* 19:183–198.
35. McGraw, C. F., A. V. Somlyo, and M. P. Blaustein. 1980. Localization of calcium in presynaptic nerve terminals. *J. Cell Biol.* 85:228–241.
36. Nicholls, D., and M. Crompton. 1980. Mitochondrial calcium transport. *FEBS Lett. (Fed. Eur. Biochem. Soc.)* 111(2):261–268.
37. Porter, K.R. 1966. Cytoplasmic microtubules and their functions. *In* Principles of Biomolecular Organization. G. E. W. Wolstenholme and M. O'Connor, editors. Ciba Foundation Symposium. Little, Brown, Boston. 308–345.
38. Rahamimoff, R. 1977. The regulation of intracellular calcium concentration and transmitter release. *Neurosci. Res. Prog. Bull.* 15(4):575–581.
39. Rakic, P. 1979. Genetic and epigenetic determinants of local neuronal circuits in the mammalian central nervous system. *In* The Neurosciences Fourth Study Program. The MIT Press, Cambridge, MA. p. 109.
40. Rice, R. V., P. F. Roslansky, N. Pascoe, and S. M. Houghton. 1980. Bridges between microtubules and neurofilaments visualized by stereoelectron microscopy. *J. Ultrastruct. Res.* 71:303–310.
41. Sasaki, S., J. K. Stevens, and N. Bodick. 1983. Serial reconstruction of microtubular arrays within dendrites of the cat retinal ganglion cell: the cytoskeleton of a vertebrate dendrite. *Brain Res.* 259:193–206.
42. Schwartz, M., and B. W. Agranoff. 1981. Outgrowth and maintenance of neurites from cultured goldfish retinal ganglion cells. *Brain Res.* 206:331–343.
43. Sokal, R. R. and F. J. Rohlf. 1981. Biometry. 2nd Ed. W. H. Freeman and Co., San Francisco.
44. Stevens, J. K., T. L. Davis, N. Friedman, and P. Sterling. 1980. A systematic approach to reconstructing microcircuitry by electron microscopy of serial sections. *Brain Res. Rev.* 2:265–293.
45. Stevens, J. K., and J. Trogadis. 1984. Computer assisted reconstruction from serial electron micrographs: a tool for the systematic study of neuronal form and function. *Adv. Cell. Neurobiol.* 5:341–369.
46. Voter, W. A., and H. P. Erickson. 1982. Electron microscopy of MAP2 (Microtubule associated protein 2). *J. Ultrastruct. Res.* 80(3):374–382.
47. Wuerker, R. B., and J. B. Kirkpatrick. 1972. Neuronal microtubules, neurofilaments, and microfilaments. *Int. Rev. Cytol.* 33:45–75.
48. Wolosewick, J. J. and K. R. Porter. 1979. Microtrabecular lattice of the cytoplasmic ground substance. Artifact or reality? *J. Cell Biol.* 82:114–139.
49. Yamada, K. M., B. S. Spooner, and N. K. Wessells. 1970. Axon growth: roles of microfilaments and microtubules. *Proc. Natl. Acad. Sci. U.S.A.* 66:1206–1212.
50. Yamada, K. M., B. S. Spooner, and N. K. Wessells. 1971. Ultrastructure and function of growth cones and axons of cultured nerve cells. *J. Cell Biol.* 49:614–635.
51. Zenker, W., and E. Hohberg. 1973. A Alpha-nerve fiber number of neurotubules in the stem fiber and in the terminal branches. *J. Neurocytol.* 2:143–148.
52. Zingheim, H.-P., W. Herzog, and K. Weber. 1979. Differences in surface morphology of microtubules reconstituted from pure brain tubulin using two different microtubule-associated proteins: the high molecular weight MAP2 proteins and tau proteins. *Eur. J. Cell Biol.* 19:175–183.